Three-dimensional optical topography of brain activity in infants watching videos of human movement

Teresa Correia[1(a)], Sarah Lloyd-Fox[2], Nick Everdell[1], Anna Blasi[3], Clare Elwell[1], Jeremy C Hebden[1] and Adam Gibson[1]

[1]Department of Medical Physics and Bioengineering, University College London, Gower Street, London WC1E 6BT, UK

[2]Centre for Brain and Cognitive Development, Henry Wellcome Building, Birkbeck College, Malet Street, London WHE 7HX, UK

[3]Department of Forensic and Neurodevelopmental Science, Institute of Psychiatry, Kings College London, UK.

(a) email tcorreia@cs.ucl.ac.uk

Abstract: We present 3D optical topography images reconstructed from data obtained previously while infants observed videos of adults making natural movements of their eyes and hands. The optical topography probe was placed over the temporal cortex, which in adults is responsible for cognitive processing of similar stimuli. Increases in oxyhaemoglobin were measured and reconstructed using a multispectral imaging algorithm with spatially variant regularisation to optimise depth discrimination. The 3D optical topography images suggest that similar brain regions are activated in infants and adults. Images were presented showing the distribution of activation in a plane parallel to the surface, as well as changes in activation with depth. The time-course of activation was followed in the pixel which demonstrated the largest change, showing that changes could be measured with high temporal resolution. These results suggest that infants a few months old have regions which are specialised for reacting to human activity, and that these subtle changes can be effectively analysed using 3D optical topography.

Keywords: optical topography, functional imaging, infant, human actions, biological motion

1. Introduction

Optical topography is a non-invasive imaging technique that uses near-infrared light to measure changes in brain activity (Gibson and Dehghani 2009, Durduran *et al*. 2010, Quaresima *et al*. (in press)). It is well suited to studying early brain development, as it can be used on alert, moving infants due to its portability, non-invasiveness and low sensitivity to movement. Moreover, the information provided by optical topography, i.e., changes in oxy- and deoxy-haemoglobin concentration ([HbO_2] and [HHb]), is physiologically relevant and cannot be obtained by any other imaging modality.

In the adult brain, certain regions are known to be involved in the perception of social and human action cues (Overwalle 2009). However, imaging modalities such as functional magnetic resonance imaging (fMRI) and positron emission tomography (PET), which have successfully been used to study the adult brain, have factors that restrict their use with awake infants. We have used our own optical topography system (Everdell *et al*. 2005) to investigate cortical responses in young infants watching videos showing human action. We observed an increase in [HbO_2] in the posterior superior temporal region bilaterally, when visual human dynamic stimuli (such as nursery rhymes), but not visual non-human dynamic stimuli, were presented to five-month-old infants (Lloyd-Fox *et al*. 2009). Recently, we investigated cortical responses to the perception of simple eye, hand and mouth movements (Lloyd-Fox *et al*. 2011). This work was motivated by recent fMRI research in adults, which found different patterns of cortical responses to different forms of human actions (Pelphrey *et al*. 2005; Thompson *et al*. 2007) in the frontal and temporal cortices. Our study, using multi-channel near infrared spectroscopy (NIRS), found similar evidence of different patterns of frontal and posterior temporal cortical activation in infants according to the type of human action being watched. However, these and related NIRS studies treat the data as single source-detector (channel) haemodynamic responses, even if the data are measured from multiple channels at different separations. We have previously shown that certain stimuli produce a response in source-detector pairs that interrogate deeper regions of the cortex, whereas others activate more superficial regions (Blasi *et al*. 2007). In this paper, we extend our previous work (Lloyd-Fox *et al*. 2011) by reconstructing images of data which we previously analysed as single-channel NIRS measurements.

Numerous research groups have produced optical images of brain activity. The first method, pioneered by researchers at Hitachi Medical Co., assumes that a change in intensity measured by a given source-detector pair has its origin midway between the source and detector, and there is no attempt to resolve in the depth direction (Taga *et al.* 2003). This approach limits the lateral

spatial resolution to the optode separation (Yamamoto *et al.* 2002). Researchers have also developed methods for reconstructing data from multiple source-detector separations and have produced 3D topographic images (Bluestone *et al.* 2001) with increasingly high spatial resolution and some depth discrimination (Zeff *et al.* 2007, White and Culver 2009) and have begun to investigate incorporating anatomical models into the image reconstruction (Custo *et al.* 2010).

There is confusion in the literature over the terminology used to describe diffuse optical imaging (DOI). We take this opportunity to clarify in some detail the terms used by our research group at UCL, in the hope that this will encourage discussion and consensus within the DOI community.

We distinguish between *topography* and *tomography* based on the purpose of carrying out the experiment. If the experimenter intends to reconstruct a 3D volume using widely spaced optodes and (crucially) attempts to measure light which has travelled through the centre of the object, then we call this *optical tomography*. This is directly analogous to X-ray computed tomography and generates 3D images where the spatial resolution in all three directions is similar. If, on the other hand, the intention is to measure activity from an array placed over a small portion of the head from close-by sources and detectors with limited depth discrimination and good temporal resolution, then we call this *optical topography*. This is analogous to topographic mapping (e.g. from satellites), where longitude and latitude are mapped accurately but altitude may be found less accurately and over a smaller range. Using this terminology, optical topography may use many overlapping sources and detectors but if they are all on the same side of the object being imaged, the depth discrimination will be poor compared to the lateral resolution, so we would not refer to it as tomography. Using this terminology, *cortical mapping* is the same technique as optical topography but we would restrict its use to functional brain studies.

In this paper, we reconstruct 3D optical topography images from data which were previously analysed as single channel NIRS measurements (Lloyd-Fox *et al.* 2011). We examine whether images reconstructed of subtle changes in alert infants provide additional information beyond that which can be obtained by analysing the single channel measurements alone. We use a new image reconstruction algorithm which reconstructs directly for chromophore concentrations from dual-wavelength data, and which uses spatially variant regularisation to enhance the depth discrimination. Note that we are not imaging visual activation in the visual cortex; rather, we are attempting to image the cognitive processing of visual activity in the temporal cortex. Our previous work showed that these areas do show activation in infants. Here, we present images of that activity for the first time.

2. Methods

2.1 Protocol

The data sample of 13 five-month-old infants was taken from the previously published data set of Lloyd-Fox *et al*. (2011), where the experimental paradigm and psychological rationale for the work are explained in detail. Briefly, the infants sat on their parent's lap while the stimuli were displayed on a screen. The experiment consisted of three different videos of human action stimuli performed by female actors either performing hand games, making silent mouth movements or looking to the left and right. The baseline or reference condition consisted of videos of non-human motion (rotating toys, cogs and pistons). In this paper, we emphasise the image reconstruction aspects of the work by concentrating on the hand and eye conditions only.

For each experimental trial, a stimulus with a duration of 10 s was alternated with a 10 s baseline measurement. These durations are shorter than are often used in adult studies to reduce the total experiment time to one which the infants tolerate with minimum movement. The stimulus does generally appear to return to baseline in this relatively short period, but it may reduce the reliability of the temporal behaviours of [HbO_2] and [HHb] in this work. The three experimental conditions were displayed pseudo-randomly to avoid anticipatory effects, but over 12 trials, an equal number of trials per condition were displayed. Trials where infants failed to look at the stimuli were excluded. At least three valid trials were required for an infant to be included in the study.

2.2 Data acquisition and processing

The UCL optical topography system (Everdell *et al.* 2005), which emits at wavelengths of 770 nm and 850 nm, was used for the data acquisition. The sources are frequency modulated and illuminated simultaneously. The photodetector output signal is then processed by a fast Fourier transform algorithm, allowing the contribution from each individual source to be recovered. Using this method, imaging rates of 10 frames per second can be achieved.

Two optical imaging arrays were placed on each temporal lobe, each consisting of 5 sources and 5 detectors, providing a total of 19 source-detector pairs per array. Each array had 13 source-detector separations at 2 cm and six at 4.5 cm (figure 1). In five-month old infants, the surface of the temporal cortex is located approximately 0.5 cm below the surface of the scalp (Salamon *et al.19*90). If we follow the generally accepted rule that the mean penetration is about half the optode separation, we see that the smaller optode separation offers some limited cortical sensitivity, but the larger separation allows deeper regions of the cortex to be interrogated

efficiently.

The probes were placed according to anatomical landmarks which were obtained by measuring each infant's head circumference and distance between the midpoint of the forehead (glabella), ears and the lowest point of the back of the skull (inion). The midpoint of the temporal arrays was placed 11 cm from the glabella, and was approximately aligned with T3 and T4 of the 10/20 international system of EEG electrode placement on an average five-month-old infant head. The position of the array did not vary more than 1 cm across infants, since the measured distance from the glabella to the imaging array was always between 10.5 and 12 cm.

Data were acquired and low-pass filtered (cutoff frequency of 1.8 Hz) for all the trials. Then each trial was separated into blocks consisting of 4 s baseline, followed by a 10 s stimulus and a 10 s post-stimulus baseline period. Each block was detrended using a linear fit between the last 4 s of the pre-stimulus baseline and the last 4 s of the post-stimulus baseline period to remove any effects of baseline drift throughout the experiment (Blasi *et al.* 2007).

Trials for each infant and experimental condition were averaged. Subsequently, each experimental condition was averaged across all thirteen infants. This resulted in a time course for each of the three stimuli. Their respective baselines were averaged over time.

2.3 Multispectral image reconstruction

Conventional image reconstruction involves finding the optical properties of the medium from a set of measurements, which are then combined to calculate the chromophore concentrations. However, in this work, we used a multispectral method which involved reconstructing chromophore concentrations using all measurements at both wavelengths simultaneously. We assumed that the true chromophore concentrations were close to an initial estimate and any changes were small, and used a linear approximation to reconstruct the difference in chromophore concentrations. We used the Rytov approximation, meaning that we solved for changes in the log intensity (O'Leary *et al.19*95).

For two measurement wavelengths (λ_1, λ_2) and two chromophores (c_1,c_2) the linear multispectral method solves the matrix equation $\Delta A_\lambda = J\Delta c$, where $\Delta A_\lambda = [\Delta A_{\lambda 1} \Delta A_{\lambda 2}]^T$ represents the changes in the logarithm of the measured data and $\Delta c = [\Delta c_1 \ \Delta c_2]^T$ the chromophore concentration changes in µMolar (µM). For CW measurements only intensity is measured, hence changes in measured data are given by $\Delta A_\lambda = log\left(\frac{I}{I_0}\right)$, where I_0 is the baseline intensity measurement. The matrix $J = \left[J_{\lambda 1}\varepsilon_{1,\lambda 1} \ \ J_{\lambda 1}\varepsilon_{2,\lambda 1}; J_{\lambda 2}\varepsilon_{1,\lambda 2} \ \ J_{\lambda 2}\varepsilon_{2,\lambda 2}\right]$ is the Jacobian or

sensitivity matrix (in units of mm) and ε is the extinction coefficient of the corresponding chromophore (in mm^{-1} μM^{-1}). It has dimensions $2M \times 2N$, where M represents the number of measurements and N is the number of image pixels.

The Jacobian was calculated for each wavelength using the software package TOAST (Temporal Optical Absorption and Scattering Tomography) (Arridge *et al.* 2000). It uses the finite element method (FEM) to model the propagation of light through highly scattering tissue using the diffusion equation, given an estimate of the medium optical properties and optode positions. The medium is considered to be a homogeneous slab with refractive index η = 1.4, absorption coefficient μ_a = 0.038 mm^{-1} and reduced scattering coefficient μ_s' = 0.75 mm^{-1} at wavelength 770 nm and μ_a = 0.042 mm^{-1} and μ_s' = 0.71 mm^{-1} at wavelength 850 nm. Following previous work (Correia *et al.* 2010), we took μ_a to be the same as that of an adult, and since scattering is much lower for an infant brain than for an adult brain, and based on values found in the literature (Bevilacqua *et al.* 1999, van der Zee 1992), we took, μ_s' to be 1/3 of that of an adult.

A FEM mesh with 32615 nodes, 21845 elements and dimensions 120 mm x 60 mm x 40 mm was generated with the meshing software NETGEN (Schöberl 1997). In order to have equivalent contributions from all measurements, a row normalisation was performed by dividing both sides of the equation by the mean of each row of the Jacobian matrix. Also, the standard deviation σ of the log amplitude can be considered a measure of the level of confidence in the data points, so a correction was applied by dividing by σ on both sides of the equation.

Chromophore concentration changes were obtained by solving the ill-posed inverse problem using all measurements at all wavelengths simultaneously. This was achieved using Tikhonov regularisation:

$$\Delta c = (J^T J + \alpha R)^{-1} J^T \Delta A, \tag{1}$$

where R is a scalar regularisation parameter, $\alpha = diag(J^T J + \gamma)^{1/2}$ is the NOSER type regularisation parameter (Cheney *et al.* 1990, Adler *et al.* 2007), with $\gamma = \beta S_{max}^{-1}$, where β is a scaling factor and S_{max} is the maximum singular value of $J^T J$. The constant γ ensures that the regularisation parameter is never too small, and its value is approximately equal to the noise present in the data. For experimental data, β = 1 most of the time, but this parameter can be adjusted to improve contrast and resolution.

Inversion using zero-order Tikhonov regularisation, i.e. equation 1 with $\alpha = I$ where I is the identity matrix, favours high sensitivity regions. Inversion using a NOSER type regularisation can be viewed as a weighted Tikhonov regularisation, which gives uniform sensitivity and equal weights to the unknowns. We have previously shown that this approach improves sensitivity and accuracy of depth reconstruction (Correia *et al.* 2009b).

In order to find the constant regularisation parameter *R*, for each stimulus, data between 8.5 and 9.5 s after the beginning of the stimulus (corresponding to a point where activation was detected) were averaged. The L-curve method (Hansen 1998, Correia *et al.* 2009a) is usually our method of choice to determine the constant regularisation parameter *R*. However, the L-curve method fails to find a regularisation parameter when the problem is normalised by the standard deviation of the data and row normalisation is applied, possibly because the problem then becomes less ill-conditioned. Nevertheless, an alternative generalised cross-validation method (GCV) (Golub *et al.* 1979, Correia *et al.* 2009a) successfully finds a regularisation parameter despite normalisation. We find that images are generally superior when normalisation is implemented, so here we used GCV to find *R*.

3. Results

3.1 Overview

3D optical topography images were reconstructed for changes in [HbO_2] and [HHb], for hand and eye stimulation. However, particularly in infant research, changes in [HbO_2] tend to be more robust and reliable indicators of functional activity than those of [HHb] (Lloyd-Fox *et al*. 2010, Watanabe *et al*. 2010, Quaresima *et al*. 2011). Therefore, haemodynamic maps shown in this section (Figures 2-3) correspond to the temporal evolution of [HbO_2] in μM. We identify the depth where the maximum change was observed and display images reconstructed on both sides of the head at that same depth (7mm for hand stimulation and 9mm for eye). Images are displayed with the posterior temporal area on the left and anterior area on the right. The dashed lines indicate the region covered by the probe. The 3D nature of the images is emphasised by displaying images of [HbO_2] as slices oriented perpendicular to the probe for both conditions (Figures 4-5), while the extent of the temporal and physiological data we obtain in [HbO_2] and [HHb] is shown by tracking a single pixel over time (Figures 6-7). Videos of the reconstructed images are available as online supplemental information.

3.2 Infants observing hand movements

Figure 2 shows *xy* cross-sections at $z = 7 \pm 1$ mm (error corresponds to half the pixel size)

through reconstructed images of changes in [HbO_2], when infants watched videos of hand movement. The stimulus was initiated at 0 s and ends at 10 s, and is followed by 10 s rest. On both sides, the maximum change in [HbO_2] is an increase which occurs 5-10 s post stimulus onset. Changes occur bilaterally, but the maximum change on the right side was 1.29 µM compared to 1.15 µM on the left.

3.3 Infants observing eye movements

Figure 3 shows *xy* cross-sections at $z = 9 \pm 1$ mm through images of changes in [HbO_2] when infants watched videos of eye movements between 0 and 10 s. Again, increases in [HbO_2] occur during the stimulus, as expected. The changes on both sides appear to be somewhat more central than in the previous condition. Examination of images taken at intermediate timepoints suggests that a stronger, faster and longer response to the stimuli occurs in the right hemisphere compared to the left hemisphere (see videos in supplemental material). In the right hemisphere, the largest [HbO_2] change was 1.96 µM while in the left hemisphere it was 1.72 µM.

3.4 Depth discrimination

In order to demonstrate the capability of the system and the image reconstruction algorithm to distinguish between events at different depths, Figures 4 and 5 show slices which are perpendicular to the face of the imaging array, extending to a depth of 20 mm below the surface. Figure 4 is a slice taken through the right hemisphere as the infants watched hand movements at the time where the maximum activation was observed, and Figure 5 is the equivalent figure for activation while the infants watched eye movements.

Both figures show some activation at depth and some activation extending up towards the surface. This is more obvious in Figure 4. Figure 5 shows a similar superficial signal but also a more substantial change occuring 7-12 mm below the surface. The activation extending to the surface may be due to stimulus-related surface effects (such as changes in scalp blood flow), or could indicate artefacts caused by imperfect coupling of the light into the head.

3.5 Time-course of physiological signal

In order to illustrate the similarities and differences in response times of [HbO_2] and [HHb], averaged haemodynamic response curves were obtained for the two experimental conditions, by following the pixel with maximum concentration change. Figure 6 shows the haemodynamic response curves of the right temporal lobe while the group of infants observed hand movements. The response times of [HbO_2] and [HHb] are quite similar, but [HbO_2] increases by an amount about four times larger than the decrease which occurs in [HHb]. An initial dip in [HbO_2] can be

seen. Figure 7 shows the equivalent graphs obtained while infants observed eye movements. For this case, the response of [HHb] is again about four times smaller than the response of [HbO_2] but in this case both demonstrate increases in chromophore concentration.

4. Discussion

It is evident that optical topography can measure and provide images of visually induced haemodynamic activity in regions of the infant brain which correspond with those parts of the brain which are activated by human action stimuli in adults. Imaging arrays were placed over both temporal lobes and images of [HbO_2] changes were successfully reconstructed, for different experimental conditions.

3D optical topography images (Figures 2 and 3) show that the cortical processing of hand movements occurs in more posterior brain regions than that of eye movement. This agrees with the NIRS study by Lloyd-Fox *et al* (2011) from which this data is derived, which showed an increase in [HbO_2] during the eye condition which was anterior to that seen during the hand condition. Similarly, both studies report bilateral activation with greater amplitude on the right side than the left. However, to make a more precise statement about anatomical activation, we need to register the optical topography images onto an anatomical image (or atlas) such as may be obtained by MRI. At the moment, this is challenging as we have no control points in common between the optical imaging array, the head and the anatomical image, but future work aims to provide such points. It is unclear how best to do this in this population as additional setup time, or the presence of markers on the head, may irritate the infant and cause more movement.

Each image is effectively a multi-dimensional array of data (a 120 x 60 x 40 mm 3D image, at 200 time points, of three chromophores, on two contralateral cortices), and there is no efficient way to display that data without losing information. We have chosen four representations here: 2D slices at a single depth at different time points, 2D slices orthogonal to the imaging array, 1D traces of the chromophore concentration over time and movies in the online supplemental information. None of these representations are ideal; the information from each is complementary but some is still lost.

The depth images (Figure 4 and 5) are informative and provide information which cannot be obtained from multi-channel NIRS measurements. In particular, such images may allow surface artefact to be identified and rejected, and provide information about the depth at which different activations occur. We observed haemodynamic activity to a depth of approximately 15 mm. Assuming the thickness of extra-cerebral regions to be about 6 mm and a grey matter thickness

of 4 mm in infants of this age, this provides confirmation that superficial regions of the gyral white matter or deeper gray matter within the sulci are being imaged. We have not considered the effect of uneven sampling on depth images, although it could be significant: the middle of the arrays contains more overlapping measurements than the edges. This is likely to reduce the quality of reconstructions, particularly depth reconstructions, at the edges of the array. However, tests on tissue-equivalent phantoms have shown reliable depth discrimination (Correia *et al.* 2009b).

The time-course analysis (Figures 6 and 7) looks similar to the analysis provided by NIRS, but we hypothesise that a time-course taken from a pixel in the reconstructed image should be a more reliable indicator of haemodynamics than one taken from analysing unreconstructed data. It should have less contamination from surface layers, it is effectively averaged over many measurements, and it should be less affected by the partial volume effect. This latter point is somewhat supported by the marginal increase in magnitude of the change reported in Figures 6 and 7 compared to the changes measured in our previous work (Lloyd-Fox *et al.* 2011). We measured changes of 1.29 and 1.96 µM for the hand and eye conditions respectively, compared to 1.2 and 1.5 µM measured using NIRS.

We observed an initial decrease in [HbO_2] (and increase in [HHb]) when the infant was presented with videos of eye movement, but not with hand movement. Some other NIRS studies (*e.g.* Gallagher *et al.* 2008, Minagawa-Kawai *et al.* 2011) have seen this dip, and it has been observed in the blood oxygen level dependent (BOLD) signal in fMRI studies. However, this initial dip, which some researchers attribute to rapid oxygen consumption at the site of activation, remains controversial in both the NIRS/optical imaging and fMRI communities because it is not always found. This topic has been widely discussed and reviewed (Yacoub *et al.* 2001, Hillman 2007, Uludağ 2010).

The controversy over the initial dip suggests that our observation that it appears to be present in some circumstances but not others, may have some truth. However, in common with other NIRS and optical topography researchers, we cannot exclude the hypothesis that some changes present in the [HHb] images can be due to cross-talk or just noise. Changes in [HHb] are quite small and the quality of the measured data can deteriorate due to averaging over infants and trials, and thus the fluctuations in activity may reflect noise. Computer simulation suggests that [HbO_2] may be overestimated by 15 % and [HHb] by 10 % (Correia *et al.* 2010).

5. Conclusions

We have demonstrated that state-of-the-art optical topography systems, coupled with

sophisticated data analysis and image reconstruction can provide a practical tool which can be used to answer genuine research questions in developmental psychology. We suggest that the additional information provided by imaging allows conclusions to be drawn from the data which are beyond those that can be obtained by multi-channel NIRS measurements alone.

Our results suggest that five-month-old infants already have specialised regions for processing human action stimuli. To our knowledge this is the first time that optical topography images of the temporal cortex have been reconstructed showing cognitive activation in this age group, which is difficult to study using other imaging modalities. We have also demonstrated the use of a sophisticated linear reconstruction algorithm on data which were obtained during subtle stimuli in a challenging study group. Optical topography potentially provides a robust method for studying cognitive development.

6. Acknowledgements

The authors would like to thank all of the parents and their infants who participated in the study. The work was supported by Fundação para a Ciência e a Tecnologia, Portugal, ECs seventh framework programme (FP7-HEALTH-2007-201076) and EPSRC (EP/F01208X/1).

7. References

A Adler, T Dai, and WRB Lionheart. Temporal image reconstruction in electrical impedance tomography. *Physiological Measurement*, 28:S1–S11, 2007.

SR Arridge, JC Hebden, M Schweiger, FEW Schmidt, ME Fry, EMC Hillman, H Dehghani, and DT Delpy. A method for three-dimensional time-resolved optical tomography. *International Journal of Imaging Systems and Technology*, 11:2–11, 2000.

F Bevilacqua, D Piguet, P Marquet, JD Gross, BJ Tromberg, and C Depeursinge. In vivo local determination of tissue optical properties: Applications to human brain. *Applied Optics*, 38(22): 4939-50, 1999.

A Blasi, S Fox, N Everdell, A Volein, L Tucker, G Csibra, AP Gibson, JC Hebden, MH Johnson, and CE Elwell. Investigation of depth dependent changes in cerebral haemodynamics during face perception in infants. *Physics in Medicine and Biology*, 53(27): 6849-64, 2007.

AY Bluestone, G Abdoulaev, CH Schmitz, RL Barbour, and AH Hielscher. Three-dimensional optical tomography of hemodynamics in the human head. *Optics Express*, 9(6):272–286, 2001.

M Cheney, D Isaacson, JC Newell, S Simske, and JC Goble. NOSER: an algorithm for solving the inverse conductivity problem. *International Journal of Imaging Systems and Technology*, 2:66–75, 1990.

A Corlu, R Choe, T Durduran, K Lee, M Schweiger, SR Arridge, EMC Hillman, and AG Yodh. Diffuse optical tomography with spectral constrains and wavelength optimization. *Applied Optics*, 44(11):2082–2093, 2005.

T Correia, A Gibson, M Schweiger, and J Hebden. Selection of regularization parameter for optical topography. *Journal of Biomedical Optics*, 14:034044, 2009a.

T Correia, A Banga, NL Everdell, AP Gibson, and JC Hebden. A quantitative assessment of the depth sensitivity of an optical topography system using a solid dynamic tissue-phantom. *Physics in Medicine and Biology*, 54:6277–6286, 2009b.

T Correia, A Gibson, and J Hebden. Identification of the optimal wavelengths for optical topography: a photon measurement density function analysis. *Journal of Biomedical Optics*, 15:056002, 2010.

A Custo, DA Boas, D Tsuzuki, I Dan, R Mesquita, B Fischl, WEL Grimson, and W Wells.

Anatomical atlas-guided diffuse optical tomography of brain activation. *NeuroImage*, 49:561–567, 2010.

T Durduran, R Choe, W B Baker and A G Yodh. Diffuse optics for tissue monitoring and tomography *Rep. Prog. Phys.* **73** 076701, 2010

NL Everdell, AP Gibson, IDC Tullis, JC Hebden, and DT Delpy. A frequency multiplexed near infrared topography system for imaging functional activation in the brain. *Review of Scientific Instruments*, 76:093705, 2005.

A Gallagher, D Bastien, I Pelletier, P Vannasing, A D Legatt, S L Moshé, R Jehle, L Carmant, F Lepore, R Béland, and M Lassonde. A noninvasive, presurgical expressive and receptive language investigation in a 9-year-old epileptic boy using near-infrared spectroscopy. *Epilepsy & Behavior*, 12:340–346, 2008.

A Gibson and H Deghani. Diffuse optical imaging. *Phil Trans R Soc A* **367**, 3055-3072, .2009

G Golub, M Heath, and G Wahba. Generalized-cross validation as a method for choosing a good ridge parameter. *Technometrics*, 21(2):215–223, 1979.

PC Hansen. Rank-deficient and discrete ill-posed problems: numerical aspects of linear inversion. *Society for Industrial and Applied Mathematics*, Philadelphia, USA, 1998.

E M C Hillman. Optical brain imaging in vivo: techniques and applications from animal to man. *Journal of Biomedical Optics*, 12(5):051402, 2007.

S Lloyd-Fox, A Blasi, A Volein, N Everdell, CE Elwell, and MH Johnson. Social perception in infancy: A near infrared spectroscopy study. *Child Development*, 80(4):986–999, 2009.

S Lloyd-Fox, A Blasi, and C Elwell. Illuminating the developing brain: the past, present and future of functional near infrared spectroscopy. *Neuroscience and Biobehavioral reviews*, 2010.

S Lloyd-Fox, A Blasi, N Everdell, CE Elwell, and MH Johnson. Selective cortical mapping of biological motion processing in young infants. *Journal of Cognitive Neuroscience*, **23**(9), p2521-2532, 2011.

Y Minagawa-Kawai, H van der Lely, F Ramus, Y Sato, R Mazuko, and E Dupoux. Optical brain imaging reveals general auditory and language-specific processing in early infant development. *Cerebral Cortex*, 21:254–261, 2011.

MA O'Leary, DA Boas, B Chance, and AG Yodh. Experimental images of heterogeneous turbid media by frequency domain diffusing photon tomography. *Optics Letters*, 20:4268, 1995.

F Overwalle. Social cognition and the brain: A meta-analysis. *Human Brain Mapping*, 30:829–858, 2009.

KA Pelphrey, JP Morris, CR Michelich, T Allison, and G McCarthy. Functional anatomy of biological motion perception in posterior temporal cortex: A fMRI study of eye, mouth and hand movements. *Cerebral Cortex*, 15:1866–1876, 2005.

Quaresima V, Bisconti S and Ferrari M. A brief review on the use of functional near-infrared spectroscopy (fNIRS) for language imaging studies in human newborns and adults, *Brain and Language*, in press

G Salamon, C Raynaud, J Regis, and C Rumeau. *Magnetic resonance imaging of the pediatric brain*. New York, NY: Raven Press. 1990

J Schöberl. Netgen - an advancing front 2D/3D-mesh generator based on abstract rules. *Computing and Visualization in Science*, 1:41–52, 1997.

G Taga, K Asakawa, a Maki, Y Konishi, and H Koizumi. Brain imaging in awake infants by near-infrared optical topography. *Proceedings of the National Academy of Sciences*, 100(19):10722–10727, 2003.

JC Thompson, JE Hardee, A Panayiotou, D Crewther, and A Puce. Common and distinct brain activation to viewing dynamic sequences of face and hand movements. *NeuroImage*, 37:966–973, 2007.

K Uludağ. To dip or not to dip: reconciling optical imaging and FMRI data. *PNAS*, 107(6):E23, 2010.

P van der Zee. Measurement and modelling of the optical properties of human tissue in the near-infrared. *PhD thesis*, University College London (University of London), 1992.

Watanabe H, Homae F, Taga G. General to specific development of functional activation in the cerebral cortexes of 2- to 3-month-old infants, *NeuroImage*, 50(4) p1536-1544 2010.

B R White and J P Culver. Phase-encoded retinotopy as an evaluation of diffuse optical neuroimaging. *NeuroImage*, 49(1) 568-577 2009.

E Yacoub, A Shmuel, J Pfeuffer, P Van De Moortele, G Adriany, K Ugurbil, and X Hu. Investigation of the initial dip in fMRI at 7 tesla. *NMR in Biomedicine*, 14:408–412, 2001.

T Yamamoto, A Maki, T Kadoya, Y Tanikawa, Y Yamada, E Okada, and H Koizumi. Arranging optical fibres for the spatial resolution improvement of topographical images. *Physics in Medicine and Biology*, 47:3429–3440, 2002.

BW Zeff, BR White, H Dehghani, BL Schlaggar, and JP Culver. Retinotopic mapping of adult human visual cortex with high-density diffuse optical tomography. *Proceedings of the National Academy of Sciences*, 104:12169–12174, 2007.

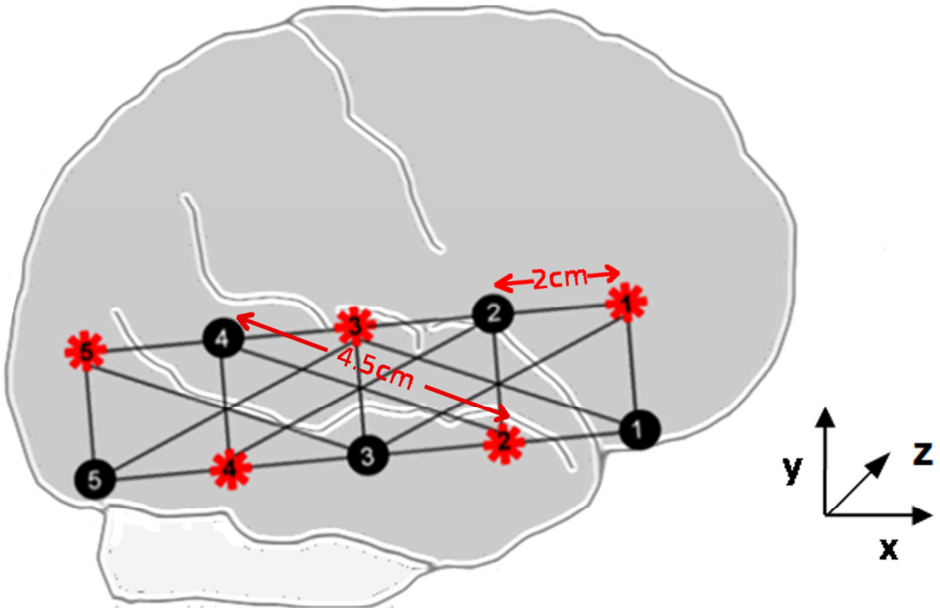

Fig 1: Schematic diagram showing the approximate position of the array on the head.

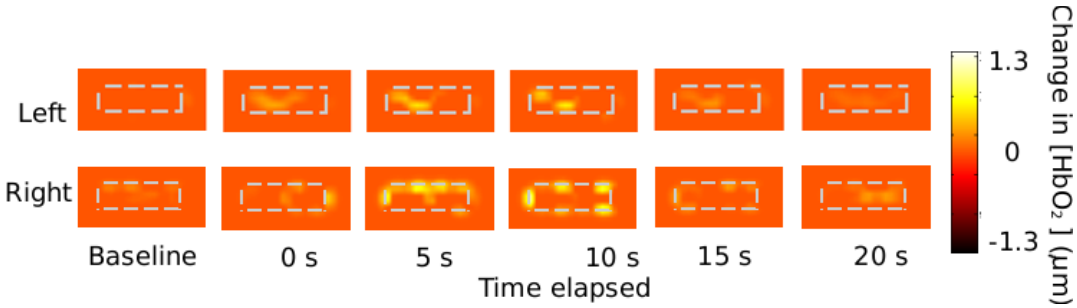

Fig 2: Reconstructed images (depth=7 ± 1 mm) of changes in [HbO_2], showing the response to the infant observing hand movements.

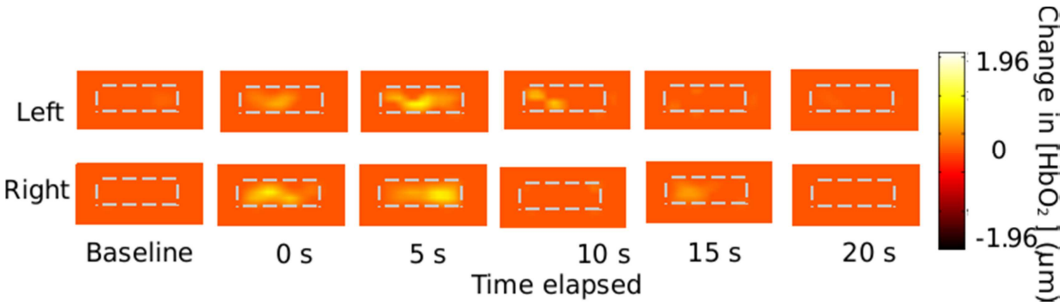

Fig 3: Reconstructed images (depth=9 ± 1 mm) of changes in [HbO_2], showing the response to the infant observing eye movements.

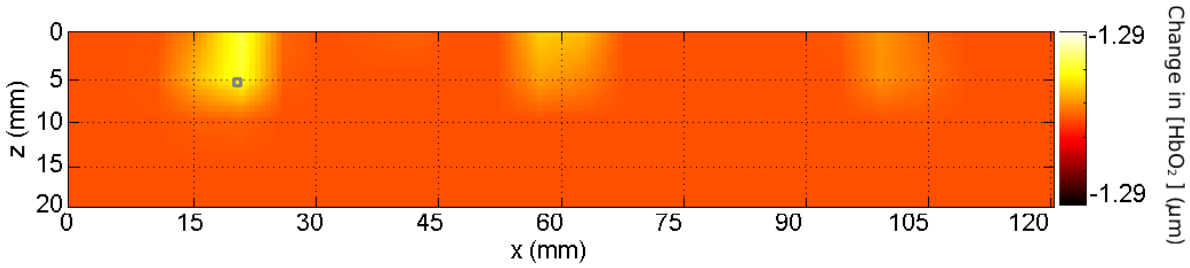

Fig 4: Depth images of changes in [HbO_2] in the right hemisphere evoked by infant observing hand movements. The square shows the pixel where the change was maximum and which was tracked to obtain the data in Figure 6.

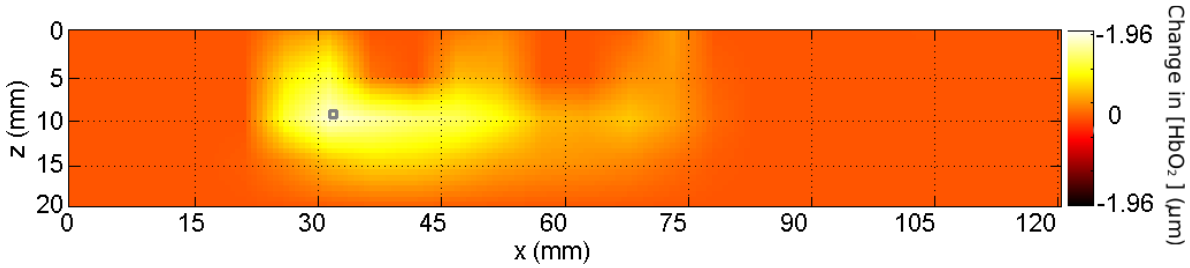

Fig 5: Depth images of changes in [HbO_2] in the right hemisphere evoked by infants observing eye movements. The square shows the pixel where the change was maximum and which was tracked to obtain the data in Figure 7.

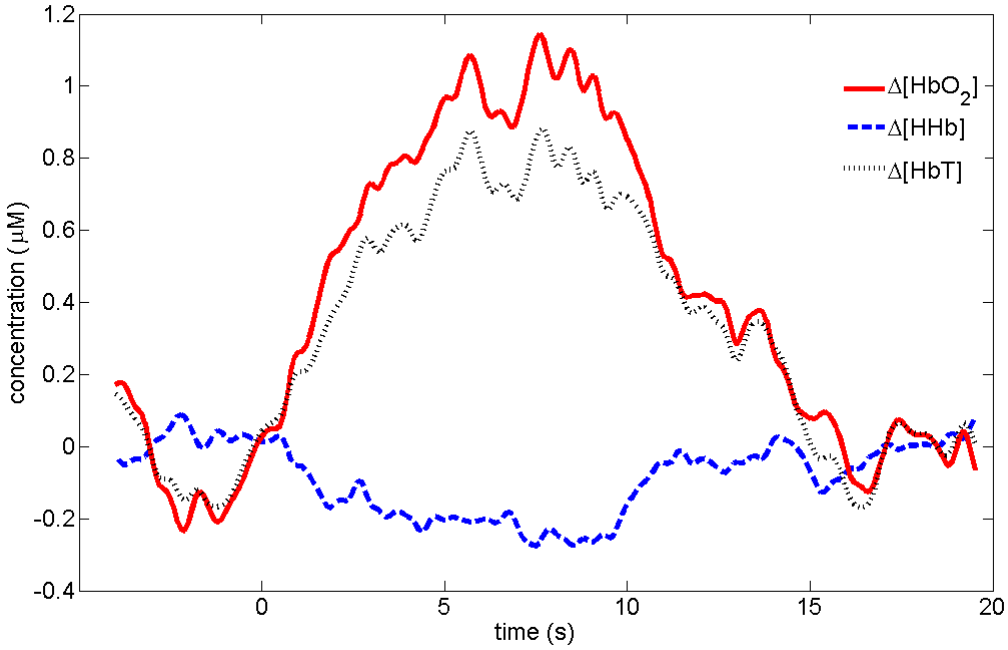

Fig 6: Haemodynamic response curves, showing changes in [HbO_2], [HHb] and total haemoglobin concentration [HbT], in the right hemisphere as infants observed videos of hand movements. The curves are taken from the pixel highlighted in Figure 4. Time *t=0* corresponds to the onset of the stimulus.

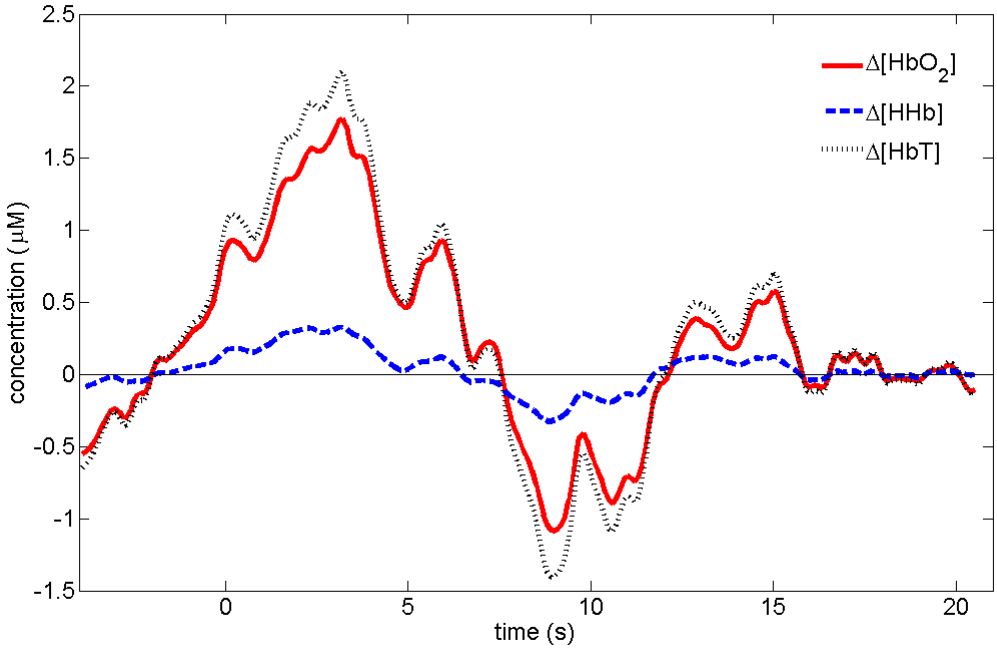

FIG. 7: Haemodynamic response curves, showing changes in [HbO_2], [HHb] and total haemoglobin concentration [HbT], in the right hemisphere while infants observed videos of eye movement. The curves are taken from the pixel highlighted in Figure 5. Time *t=0* corresponds to the onset of the stimulus.